JOURNAL OF MATERIALS SCIENCE, 30 (1995) 4651–4658

Residual thermal stresses in the pull-out specimen: a finite element calculation

F.-H. LEROY, M.-H. AUVRAY, P.-M. LESNE
Office National d'Etudes et de Recherches Aérospatiales, BP72, 92322 Chatillon Cedex, France

The residual thermal stress field in the pull-out specimen is calculated in the case of a high properties thermoset system (carbon–*bis*maleimide). The calculation is performed within the framework of the linear theory of elasticity by means of a finite element method. The specimen is modelled as a three-phase composite (holder–fibre–matrix). The meniscus which forms at the fibre entry is taken into account in order to provide a realistic stress concentration. The latter is far higher than the matrix strength. Evidence that fibre debonding propagates from the fibre end during cooling is then produced.

Nomenclature

ΔT	thermal load
L_e	embedded length
r_f	fibre radius
ρ_c	curvature radius of the meniscus (fibre entry)
r_c	radial dimension of the finite element mesh
E_m, E_h	matrix and holder moduli
E_A, E_T	fibre axial and transverse moduli
α_m, α_h	matrix and holder thermal expansion coefficients
α_A, α_T	fibre axial and transverse thermal expansion coefficients
σ_{rr}, $\sigma_{\theta\theta}$, σ_{zz}, τ_{rz}	non-zero components of the residual stress field
σ^i_{rr}, $\sigma^{im}_{\theta\theta}$, σ^{im}_{zz}, τ^i_{rz}	stresses at the interface in the matrix ($r = r_f + \varepsilon$)
σ^i_{rr}, $\sigma^{if}_{\theta\theta}$, σ^{if}_{zz}, τ^i_{rz}	stresses at the interface in the fibre ($r = r_f - \varepsilon$)
σ_{pl}	maximum principal stress
σ^f_{zz}	mean axial stress over the fibre section
σ^m_{rupt}	matrix strength
u_r, u_z	non-zero components of the displacement field

1. Introduction

Failure behaviour of unidirectional continuous-fibre composites under axial tensile load mainly arises from the way load is transferred/shared near fibre breaks. Since it usually involves fibre debonding, an interfacial failure criterion is needed for modelling purposes. Numerous researchers have managed to find such a criterion by using single embedded fibre tests.

Obviously, the more accurate the evaluation of the load carried by the interface during these tests is, the more reliable the interfacial failure criterion can be. This is why the literature abounds with "new" theoretical stress analyses of the tests. In this context, it is surprising to note that the proposed analyses, although they are often applied to high properties thermoset systems, such as C–epoxy, are still simplistic as far as residual thermal stresses (RTS) are concerned. Thus, only the components which are continuous through the interface (σ_{rr}, τ_{rz}) are evaluated in the near matrix and the maximum principal stress (σ_{pl}) is not available. Moreover, stress concentration near fibre breaks is not addressed (σ_{rr} = constant, for example).

McCartney [1] and Nairn [2], dealing with the fragmentation test, break the rule. These analytical models provide information about all the components of the residual stress field in the fibre and in the matrix, including stress concentrations.

On the other hand, no analytical solution for RTS in the pull-out specimen stands out. McCartney's and Nairn's models are not suitable for this problem, although they claim to be. Replacing the boundary conditions of the fragmentation test by those of the pull-out test, as proposed by those authors, is not adequate since these analyses are based on the restrictive assumption that the axial stress in the matrix (σ^m_{zz}) does not depend on the radial coordinate. This is, of course, wrong in the pull-out specimen.

So, we wish to point out the lack of information about RTS in the pull-out specimen. Since development of a quite rigorous analytical solution is proving a long and exacting labour, a finite element calculation is required further without delay.

Several attempts have been already made to study the pull-out test by means of the finite element method. Generally, only the stress field due to the loading of the fibre during the test [3–5] was addressed.

Nevertheless, Marotzke [6] took into account RTS in the case of a glass fibre embedded into a polycarbonate matrix. This fibre–matrix system generates low

0022–2461

RTS in comparison with stresses induced by the applied load. Therefore, results may not be representative of what occurs when thermoset systems are tested. Moreover, no information is given about residual axial and hoop stresses in the matrix near the interface. Finally, we wish to focus on two major issues:

1. Stress concentration at the embedding point is not available since the meniscus usually observed at the free surface is not modelled. In this context, the stress field is singular where the free surface joins the fibre (both phases are regarded as linear-elastic and perfectly bound) and the finite element calculation gives stresses which are mesh dependent. Marotzke has improved his model in a more recent work [7] (the meniscus was modelled), but he has no longer evaluated RTS!
2. The resin in which the fibre is embedded is usually set on a stiff holder (e.g. aluminium or steel). It may be neglected when evaluating the stress field induced by the loading of the fibre. But the holder is strongly involved in the RTS settlement [8]. The pull-out specimen must be considered as a three-phase composite material. Marotzke does not tackle this issue, nor anyone else to our knowledge.

The purpose of this paper is to focus on the RTS field arising in a pull-out specimen when high properties thermoset polymers are used. A finite element calculation is performed within the linear theory of elasticity (Section 2). A realistic meniscus is modelled at the embedding. Moreover, the matrix is assumed to be bound to an aluminium holder during cooling from the last stage of the curing cycle. We choose the T800 carbon fibre (TORAY) and a so-called thermostable resin, namely the *bis*maleimide 5250-2 (BASF). We first analysed all the components of the stress tensor, including the derived maximum principal stress, σ_{pl}, with regard to general aspects (Section 3). Influence of the holder, the meniscus and other specimen features are discussed in Section 4. Finally (Section 5), the absolute amplitude of the stresses is considered and it is proposed that: (a) an interfacial failure is initiated at the embedded end of the fibre at the onset of cooling; and that (b) a crack is propagating along the fibre until room temperature (20 °C) is reached. Experimental evidence is then provided.

2. Finite element model

2.1. Materials

An intermediate carbon fibre T800HB (diameter 5.2 μm [9]) is embedded into a *bis*maleimide (BMI) resin, namely 5250-2 (BASF product). BMI resins are characterized by a relatively high glass transition temperature (ca. 300 °C). The resin is cured on an aluminium holder. High temperatures are required during elaboration and therefore meaningful RTS are expected. More precisely, the temperature reaches 245 °C during the last stage of the 5250 curing cycle.

Materials are supposed to undergo linear-elastic strains during cooling. This is an approximation as far as the behaviour of BMI 5250 is concerned, owing to viscous effects that may be significant above 200 °C.

Mechanical properties of the three materials are summarized in Table I. Matrix and holder are assumed to be isotropic, whereas the carbon fibre is assumed to be transversely isotropic. It should be noticed that the four thermal expansion coefficients (two for the fibre) cover a large range of values (-1×10^{-6}–$50\times10^{-6}\,°C^{-1}$).

2.2. Boundary conditions

The boundary conditions are summarized in Fig. 1:

- The specimen freely shrinks in both radial and axial directions. The bottom of the holder is axially fixed;
- There is no external mechanical load. A thermal load is applied and the stress field arising from the mismatch of expansion coefficients between the three bound phases evaluated;
- The stress-free temperature is assumed to be the temperature of the last stage of the curing cycle (245 °C). Temperature is supposed to be homogeneous in the whole specimen. The calculation evaluates RTS at 20 °C ($\Delta T = -225$ °C).

Only the part of the specimen which undergoes non-homogeneous stresses due to fibre proximity is modelled. So we need: (a) to define a critical radius, r_c, beyond which the stress field in the matrix can be considered as the far-field ($\sigma_{rr} = \sigma_{\theta\theta}$ = constant, $\tau_{rz} = \tau_{r\theta} = \tau_{\theta z} = \sigma_{zz} = 0$); and (b) to apply the required boundary conditions to the edge of the modelled structure ($r = r_c$). In practice, the matrix behaves, far from the fibre and the button edge, as

TABLE I Input parameters used for the calculation, either given by the fabricant or (*) measured [9]

Property	Fibre T800HB–40B (TORAY)	Resin bismaleimide 5250-2 (BASF)	Aluminium (holder)
E_A, E_m or E_h (MPa)	294000	4200*	74000
E_T (MPa)	23000		
G_A, G_m or G_h (MPa)	25000	1500	28000
ν_A, ν_m or ν_h	0.26	0.35	0.3
ν_T	0.39		
α_A, α_m or α_h(10^{-6}, °C^{-1})	−0.9	50*	23
α_T (10^{-6}, °C^{-1})	18		
mean diameter (μm)	5.2*		

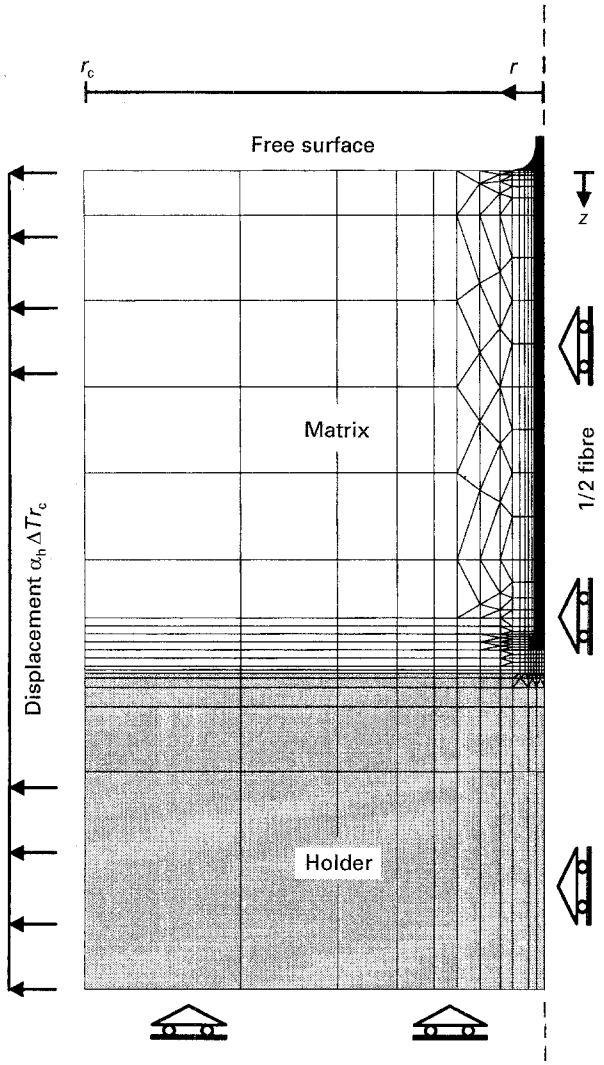

Figure 1 Finite element mesh and boundary conditions. The axis of symmetry (z), which is also the fibre axis, is on the right-hand side.

a thin layer whose radial displacement is forced by the holder shrinkage ($E_h \gg E_m$) and does not depend on the z coordinate. So we set:

$$u_r(r = r_c) = \alpha_h \Delta T r_c$$

The axial displacement is assumed to be free for $r = r_c$. The calculated stress field is proving close enough to the sought solution for $r_c = 100\, r_f$: it is hardly modified when r_c exceeds this value. In the same way, a critical thickness of the holder, which is ca. 100 μm, is defined. It should be noticed that the former boundary conditions are still adequate when the holder is also made of resin (half-infinite matrix).

2.3. Finite element mesh

It is convenient to consider that the fibre is aligned perpendicularly to the matrix-free surface. The calculation can then be performed assuming axisymmetry. The mesh (Fig. 1) contains 764 elements for an embedded length, L_e, of 150 μm (experimental range: 15–400 μm). Experimentally, L_e is controlled by varying the thickness of the layer of resin set on the holder before the fibre is embedded. However, the fibre may not stay in contact with the holder after curing.

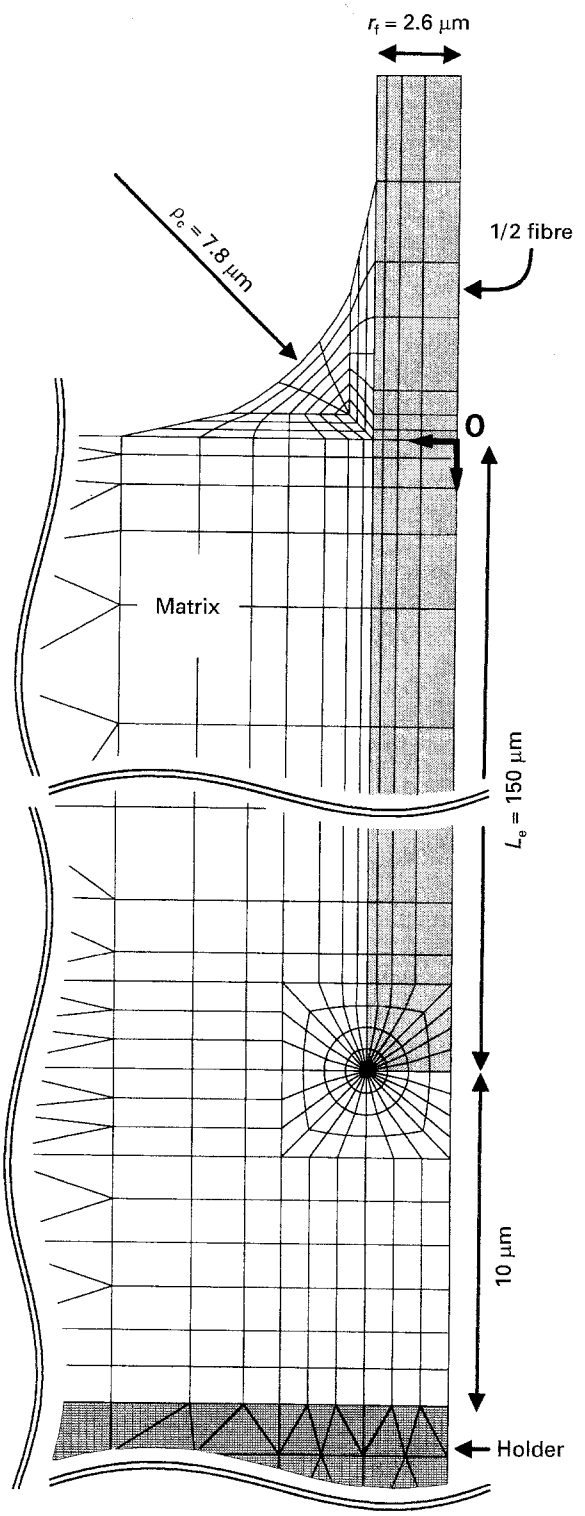

Figure 2 Details of the finite element mesh.

Therefore, it is assumed that there is, between the holder and the fibre end, a thin layer of resin whose thickness is set to 10 μm. The influence of this parameter is discussed later.

A realistic meniscus is modelled at the embedding point (Fig. 2); the curvature radius (ρ_c) is set to one-half the fibre diameter for the studied system.

The element mesh is refined where a strong gradient of the stress tensor is expected, i.e. near the fibre–matrix interface, especially in the matrix and near fibre ends (Fig. 2). Mesh independence has, of course, been verified.

3. Qualitative analysis of the residual stress field

This section deals with the residual stress field arising at the fibre–matrix interface; its components are noted with the superscript "i". Superscripts "m" and "f" are required every time the component under consideration is not continuous through the interface. The following results are obtained for $L_e = 150$ μm and 20 °C ($\Delta T = -225$ °C). We concentrate on the complexity of the stress distribution. A quantitative analysis is performed in Section 5.

3.1. General comments

The stress distribution in the matrix is highly non-homogeneous in the vicinity of the fibre (Fig. 3), due to the finite length of the embedding and to the stress concentrations located at fibre entry ($z = 0$) and fibre end ($z = 150$ μm). End effects are more or less widespread depending on the component. Radial and hoop stresses (σ^i_{rr}, $\sigma^{im}_{\theta\theta}$) exhibit sharp peaks whereas shear and axial stresses (τ^i_{rz}, σ^{im}_{zz}) are disturbed along the whole interface length.

The stress field is strongly triaxial: τ^i_{rz}, $\sigma^{im}_{\theta\theta}$, σ^i_{rr} and σ^{im}_{zz} present similar amplitudes (Fig. 3). Consequently, except for the middle part of the embedding where the principal stress $\sigma^{im}_{\theta\theta}$ is also the main load (Fig. 4), the maximum principal stress σ^{im}_{pl} is out-of-axes in the rz plane. Besides, it is much higher than the above mentioned components (about two times greater at the embedding point). It is worth noting that, although σ^{im}_{pl} exhibits a strong gradient at the extremities of the embedding, the corresponding principal direction remains quite constant and close to $z + r$ and $z - r$ near fibre entry and fibre end, respectively.

The maxima reached by stresses at the embedding point (Fig. 3) essentially depend on the curvature of the meniscus (see Section 4.2). A higher refinement of the element mesh has no significant effect on these maxima. Things do not go the same way at the fibre end: the more refined the mesh, the higher the stresses. This comes from the fact that the circular edge of the fibre is a line singularity where stresses are not bounded. It is then difficult to get reliable information about stresses arising near this line by a finite element method (see [6] for more details). However, the produced results are consistent with the theory of

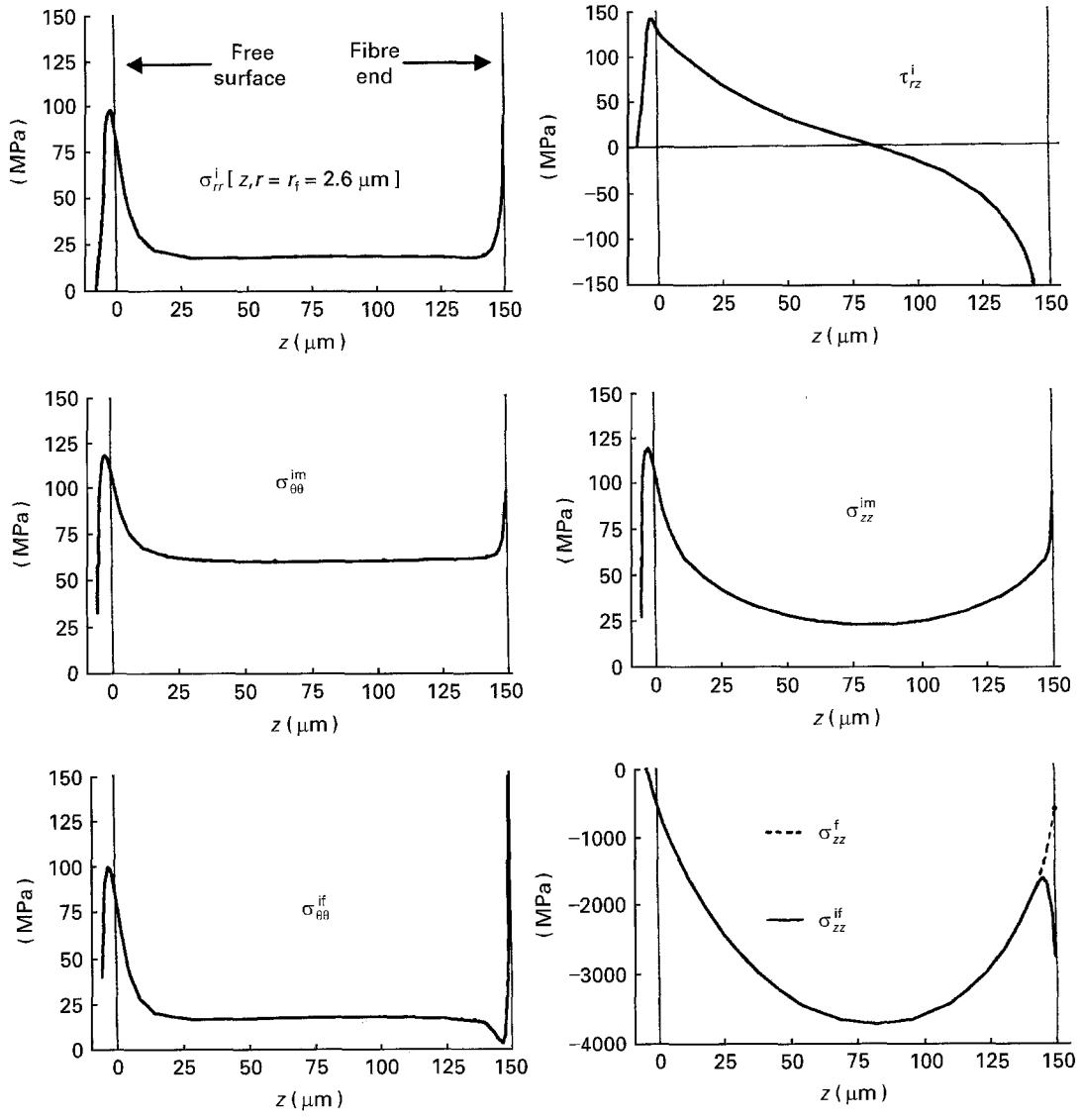

Figure 3 Residual thermal stresses along the fibre–matrix interface (T800HB–5250-2, $\Delta T = -225$ °C, $L_e = 150$ μm).

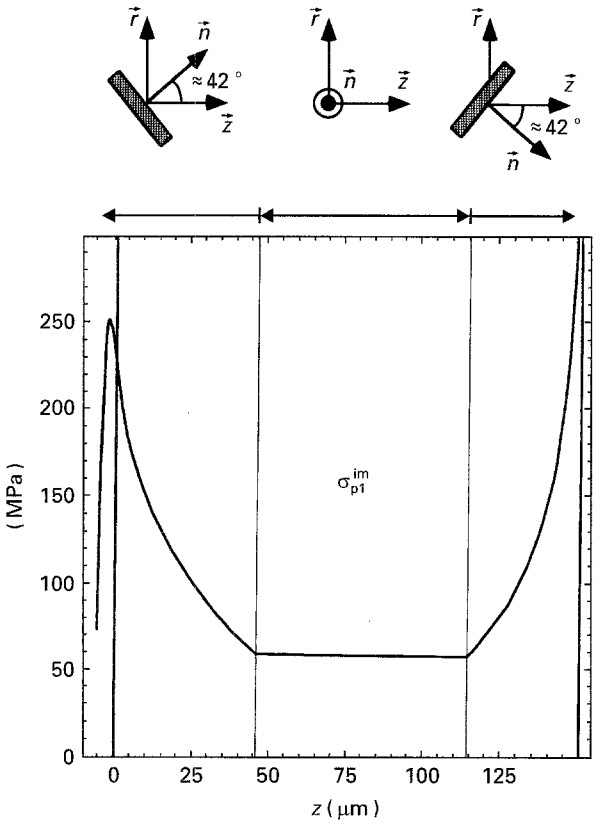

Figure 4 Maximum principal stress along the fibre–matrix interface and corresponding principal direction (T800HB–5250-2, $\Delta T = -225\,°C$, $L_e = 150\,\mu m$).

elasticity and with the idealized shape of the fibre end down to one fibre radius away from the singularity.

3.2. Interfacial shear stress

The interfacial shear stress distribution looks symmetrical (Fig. 3). This comes from the balance of the fibre in the axial direction. The force applied to the fibre end has little influence on the compression state of the fibre. Things would be the same if both fibre extremities were free. Therefore, τ_{rz}^{i} is nearly self-balanced.

End effects spread along the whole interface. Besides, τ_{rz}^{i} exhibits a rather strong, and almost constant, gradient (with respect to z) in the middle embedding. It suggests that much higher embedded lengths are required for τ_{rz}^{i} to reach the far-field solution ($\tau_{rz}^{i} = 0$, σ_{zz}^{f} = constant) away from extremities. For usual L_e values, what happens at one end of the embedding has an influence upon the stress field arising near the other one.

3.3. Interfacial axial stresses

The fibre locally prevents the matrix from contracting in the axial direction ($\alpha_A = -1 \times 10^{-6}\,°C^{-1}$). Therefore, the fibre is axially loaded in compression and the near-matrix is in tension (the whole resultant must be zero).

The stronger the action of the fibre (i.e. the higher $|\tau_{rz}^{i}|$), the more strained the matrix (i.e. the higher σ_{zz}^{im}). The axial stress, however, presents much slower variations than τ_{rz}^{i} (except near the meniscus). This damping effect is due to the fact that the axial load transferred through the interface is schematically carried by a layer of matrix whose thickness increases with τ_{rz}^{i}. What happens at the fibre entry is critical: there must be a strong jump of σ_{zz}^{im} since the radius of the resin button abruptly decays down to the small radius of the meniscus base (Fig. 2).

The axial stress is fairly homogeneous over the fibre section except near the singularity, where σ_{zz}^{if} is no longer representative of the mean stress σ_{zz}^{f} (see Fig. 3). The latter is either zero or low at fibre entry and fibre end, respectively. Its amplitude increases up to a maximum value reached near the centre of the embedding. The gradient of σ_{zz}^{f} is proportional to τ_{rz}^{i}. So, firstly, compression increases more rapidly near fibre ends than in the middle embedding. Second, there is no plateau value since τ_{rz}^{i} exhibits a non-zero gradient where it turns to negative. Third, σ_{zz}^{if} shows a parabolic shape due to the linearity of τ_{rz}^{i} in the middle embedding. It is worth noting that σ_{zz}^{f} is far greater than the other components. So the stress field arising in the fibre is almost uniaxial.

The stress distribution around the fibre end is complex (Fig. 5): the layer of matrix which separates the fibre from the holder is clipped, whereas the matrix is strongly stretched near the interface. The boundary between these two stress states is a stress-free line rising close to the singularity and going away from the fibre–matrix and matrix–holder interfaces.

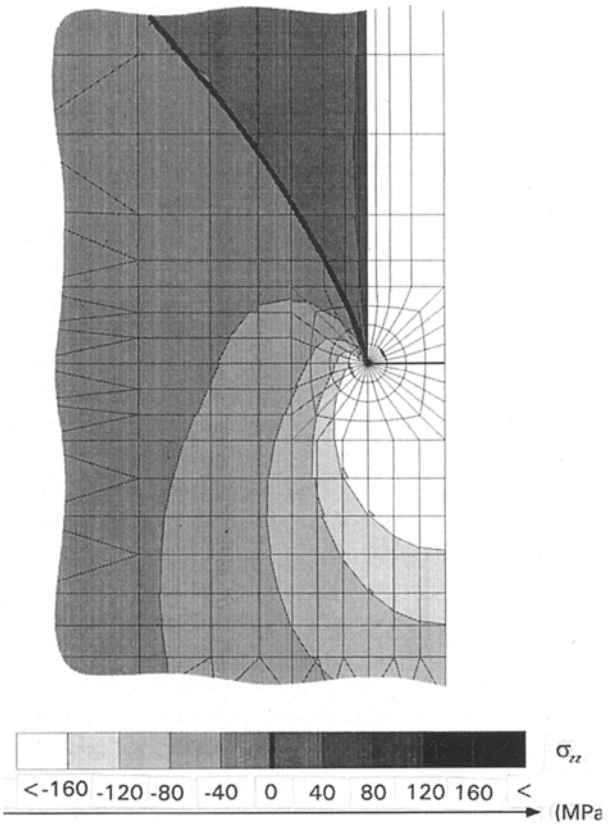

Figure 5 Residual axial stress in the vicinity of the fibre end. Matrix undergoes tension in the region delimited by the fibre–matrix interface and the stress-free line (thick line).

3.4. Interfacial radial and hoop stresses

Radial and hoop stresses are close together in the whole fibre except in a small region near the singularity (Fig. 3). The jump of $\sigma_{\theta\theta}$ through the interface is a common result as well.

On the other hand, the radial tension arising at the interface is unexpected. It is worth understanding that σ^i_{rr} is induced by both: (a) the fibre–matrix and (b) the matrix–holder thermal contraction mismatches. Mismatch (a) leads to shrinkage, whereas (b) leads to radial tension. Preponderance of (b) over (a) accounts for the calculated positive σ^i_{rr}.

A significant friction is observed after the complete failure of the interface, during the pull-out test; this seems to question the produced positive σ^i_{rr}. It should be clear that complete debonding allows axial contraction of the matrix and therefore leads to thoroughly different RTS. In particular, σ^i_{rr} turns to shrinkage. In order to account for this, let us "replace" the fibre by a hole at the onset of cooling: the hole diameter decreases during cooling by a factor of at least $\alpha_h \Delta T$ (matrix follows the holder displacement) and at most $\alpha_m \Delta T$ (matrix freely contracts), anyway by a greater factor than the fibre thermal strain ($\alpha_T < \alpha_h < \alpha_m$).

The radial stress is almost constant along the whole interface, but stress concentrations arising at both extremities can not be neglected regarding the strong influence that radial tension may have upon debonding. For example, σ^i_{rr} increases by a factor of five near the fibre entry.

4. Influence of the specimen features

4.1. Meniscus

The curvature of the meniscus depends on the fibre–matrix system. The more pronounced the curvature, the higher the stress concentration. We verified that a zero curvature radius, ρ_c, leads to unbounded stresses (singularity). We set ρ_c to one-half a fibre diameter for the system T800–BMI-5250. This is approximative since the real meniscus does not have the constant curvature assumed in Fig. 2. So, in order to get information about the influence of the curvature upon stress concentration, we modelled a meniscus with a lower ρ_c of only one fibre diameter. The shear stress is hardly affected whereas σ^i_{rr} presents an increase of ca. 15% at the fibre entry.

Stress concentration at the fibre entry is not only localized at the interface; severe stress concentrations also arise at the meniscus hollow (Fig. 6).

4.2. Holder

We have shown in the previous section that a radial tension arises at the interface instead of an expected shrinkage, due to the holder. The holder influence can be classed as a shift of the σ^i_{rr} $[z]$ curve towards positive values (Fig. 7). As a first approximation, the shift can be compared to the radial tension arising away from the fibre:

$$\Delta\sigma^i_{rr} \approx E_m(\alpha_h - \alpha_m)\,\Delta T/(1 - \nu_m)$$

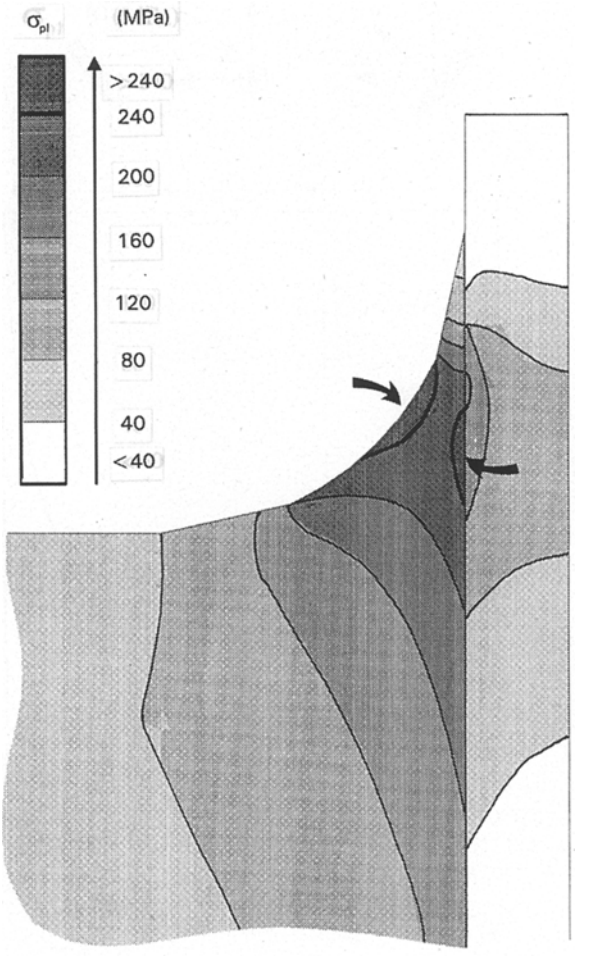

Figure 6 Maximum principal stress at the fibre entry. Localization of stress concentration at the fibre–matrix interface and at the meniscus hollow.

As a result (Poisson effect), τ^i_{rz} is ca. 70% greater than it would be if the matrix was half-infinite (resin holder).

It is worth noting that residual stresses can be controlled by choosing holders made of different materials. This is a way to modify the character of the interfacial load arising in the pull-out test, and thus to study its influence upon debonding. Let us remember that the pull-out test is used in view of determining an intrinsic debonding criterion, i.e. a criterion that is still valid in the heart of the composite where the stress field is different.

4.3. Distance between the holder and the fibre end

We used four different meshes with the distance (d) between the holder and the fibre end varying from zero to five fibre diameters ($L_e = 150$ μm). Results converge rapidly when d increases; they hardly vary for greater values than 10 μm. For lower values, one observes a decrease in the global level of τ^i_{rz} near the fibre end. It is counter-balanced by an increase of the axial force applied to the fibre extremity so that the stress field arising in the first half embedding remains unchanged.

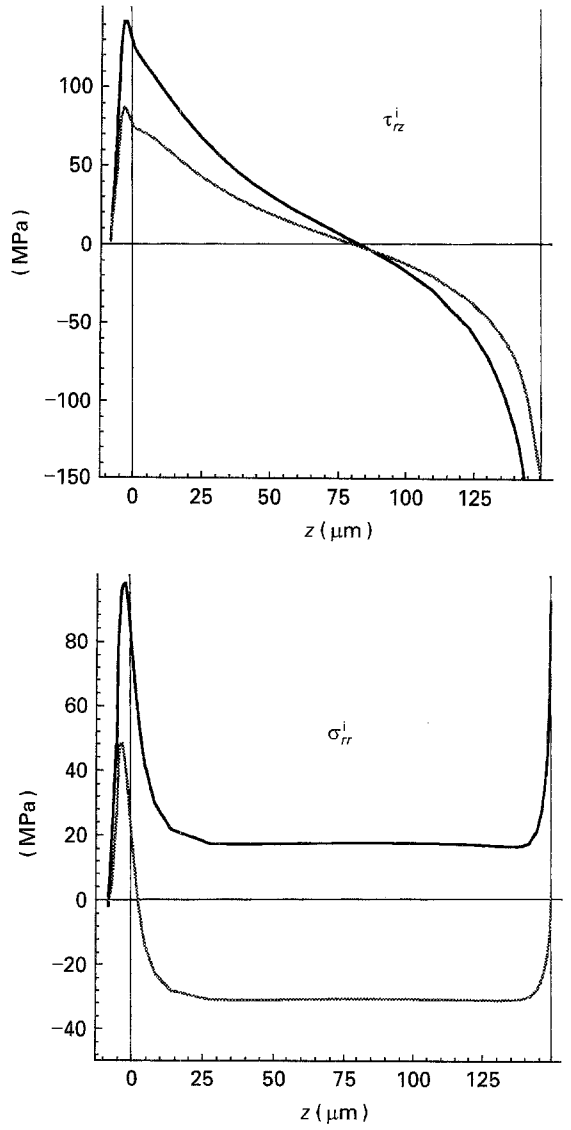

Figure 7 Influence of the holder nature upon residual shear and axial stresses at the interface: —— aluminium holder; ~~~, 5250-2 resin holder (ca. half-infinite matrix).

4.4. Embedded length

Provided results are obtained with $L_e = 150$ μm, then shorter embeddings down to 15 μm can be modelled. Results look similar except for the stress concentration at the fibre entry: the lower L_e, the lower the entry is. The correlation is strongly non-linear, i.e. concentrations rapidly decrease under 50 μm whereas they start saturating ca. 150 μm.

4.5. Fibre radius

The radius of the T800 fibre presents a significant dispersion ($r_f = 5.2 \pm 0.5$ μm, measured by scanning electron microscope). The higher r_f, the higher stress concentrations. In the specified range of values, the maxima of τ^i_{rz} and σ^i_{rr} at the fibre entry vary by ca. 10 and 20%, respectively.

5. Quantitative analysis of the residual stress field

Along the whole embedded length, σ^{im}_{p1} is higher than the matrix strength σ^m_{rupt} estimated at 60 MPa (at 20 °C) by the fabricant (see Fig. 4). The ratio $\sigma^{im}_{p1}/\sigma^m_{rupt}$ rises from ca. 1 in the middle embedding (plateau value) to > 4 near both extremities. This unrealistic result points to the fact that stresses are partially released during cooling. A calculation accounting for the non-linear behaviour of the resin is likely to lead to the same conclusion since it was verified that results would be still unrealistic if the modulus of the matrix was only half its value. So, the point is to determine which release mechanism(s) is(are) involved (viscous effects, plastification or debonding). Unfortunately, no pertinent information is available by direct observation: the pull-out specimen does not lend itself to the photoelasticimetry technique, more especially as BMI exhibit poor optical properties.

The amount of energy that must be dissipated is too important so that it could be performed through viscous mechanisms; namely the 5250-2 resin exhibits a significant viscosity only in the 200–300 °C range, as observed by di Landro and Pegoraro [9]. Yielding of the matrix is not expected in the vicinity of the fibre since BMI resins behave in a brittle way, and also since no evidence of an interphase has (up until now) been provided for the system under consideration. Finally, fibre debonding seems to be the only mechanism that is likely to dissipate the adequate amounts of energy.

It is only reasonable to assume that the edge of the fibre end is sharp enough so that the interface is locally damaged from the onset of cooling. In this context, an interfacial crack is likely to be initiated at the fibre extremity and to propagate as long as the thermal load is increasing, i.e. until 20 °C is reached. Experimental evidence of this interfacial crack is provided when differential expansion is allowed between the debound portion of the fibre and the matrix: this is achieved by separating the resin button from the holder. The fibre extremity then runs through the thin remaining layer of resin, possibly present between the fibre and the matrix, and stands out. This process was observed with INVAR alloy holders and with an embedded length of ca. 300 μm (Fig. 8); these conditions – an almost-zero holder expansion coefficient and a long embedded length – were chosen in order to emphasize RTS (see Section 4) and to obtain a more pronounced effect.

The difference of level between the free surface and the fibre end, h, provides information about the debound length, L_d. A lower bound L^*_d for L_d, that would be reached if no interfacial friction was happening, can be evaluated as follows:

$$L_d \geqslant L^*_d = h/[(\alpha_A - \alpha_m)\,\Delta T]$$

For the fibre–matrix system under consideration, L^*_d is ca. 100 times h; the difference of level between the fibre extremity and the plane-free surface observed in Fig. 8 then suggests that the fibre is at least half debonded.

In practice, separation of the resin button from the holder is obtained by decreasing the holder roughness; it originates from the differential shrinkage of the resin and the metal. Therefore, separation occurs before room temperature is reached and interfacial thermal

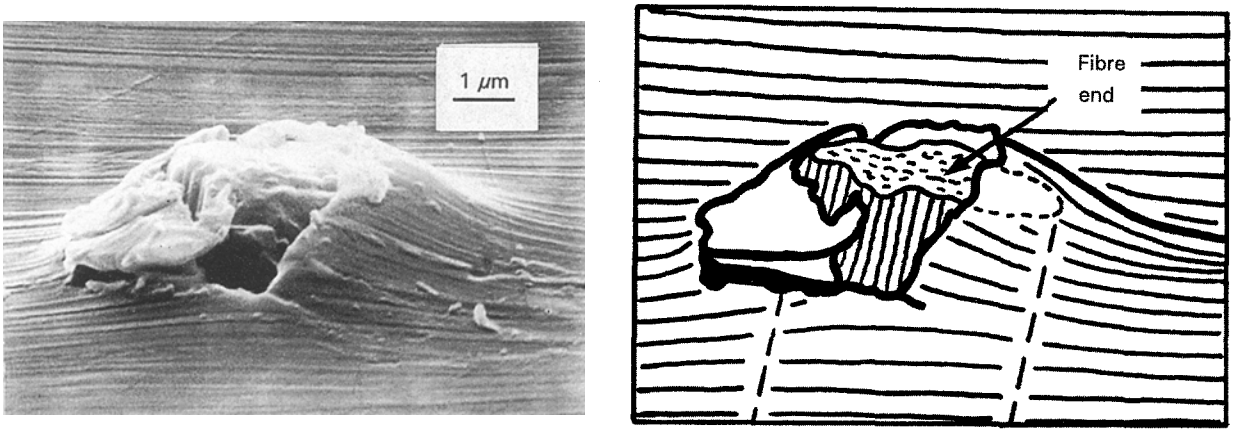

Figure 8 Evidence of fibre–matrix debonding at the fibre end: scanning electron micrograph of the hidden side of the resin button after resin–holder debonding. The fibre end runs through a thin layer of resin and stands out because of fibre–matrix debonding and differential expansion.

stresses are likely to reach much lower values than in the full pull-out specimen, i.e. with the resin still attached to the holder. In this context, large interfacial failures are likely to arise when the aluminium holder is used as well.

6. Conclusion

Residual thermal stresses (RTS) in the pull-out specimen strongly influence results of testing when high properties thermoset systems such as carbon–*bis*-maleimide are studied [8]. This raises the problem of RTS evaluation for thermoset systems in general, especially carbon–epoxy.

Investigators usually concentrate on the analytical modelling of the mechanically-loaded specimen without paying much attention to thermal loading: plane strain is commonly assumed concerning RTS. Evidence is given here that such an approximation leads to the most essential features of the residual stress field being missed. First, the whole interface undergoes shear loading due to its finite length. Second, high end effects affect all the components of the stress field. This must be all the more taken into account that the interfacial radial stress peaks in tension. Finally, RTS levels vary with the embedded length.

Besides, RTS may be high enough to cause interfacial debonding propagation from the fibre end during cooling. This damage must be limited, otherwise working out the analysis of experimental results becomes unrealistic. To this end, owing to the influence of the holder upon RTS (see Section 4.2) it is suggested that a holder with a thermal expansion coefficient greater than the thermal expansion coefficient of the matrix is used.

Acknowledgements

This work was partly supported by the EEC through a BRITE–EURAM contract and by the STPA.

References

1. L. N. McCARTNEY, *Proc. R. Soc. Lond.* **A425** (1989) 215.
2. J. A. NAIRN, *Mech. Mater.* **13** (1992) 131.
3. C. ATKINSON, J. AVILA, E. BETZ and R. E. SMELSER, *J. Mech. Phys. Solids* **30** (1982) 97.
4. J. K. MORRISON, P. S. SURENDRA and Y. S. JENQ, *J. Engng. Mech.* **114** (1988) 277.
5. M. F. MARMONIER, G. DESARMOT, B. BARBIER and J. M. LETALENET, *Journal de mécanique théorique et appliquée* **6** (1988) 741.
6. C. MAROTZKE, in Proceedings of the Second International Conference on Interfacial Phenomena in Composite Materials, Leuven, September 1991, edited by I. Verpoest and F. Jones (Butterworth-Heinemann, Oxford, 1991), p. 69.
7. *Idem.* in Proceedings of the Sixth European Conference on Composite Materials, Bordeaux, September 1993, edited by A. R. Bunsell, A. Kelly and A. Massiah (Woodhead Publishing, Abington, Cambridge, 1993), p. 281.
8. M. H. AUVRAY, P. CHENEAU-HENRY, F. H. LEROY and J. P. FAVRE, *Composites* in press (1995).
9. L. DI LANDRO and M. PEGORARO in Mid-term assessment report of BRITE EURAM contract BREU/CT91-9503 (1993).

Received 28 April 1994
and accepted 3 February 1995